Ionics (2020) 26:1181–1187
https://doi.org/10.1007/s11581-019-03272-2

ORIGINAL PAPER

Flower-like $Li_{0.36}V_6O_{13}$ with superior cycling stability as a cathode material for lithium-ion batteries

Ting-ting Lv[1] · Zheng-guang Zou[1] · Yan-wei Li[1] · Shu-chao Zhang[1]

Received: 19 June 2019 / Revised: 20 September 2019 / Accepted: 22 September 2019 / Published online: 26 November 2019

Abstract

3D flower-like $Li_{0.36}V_6O_{13}$ has been fabricated via a facile solvothermal method using C_2H_5OH, V_2O_5, and $LiNO_3$ as raw materials. The microstructure of the sample was characterized by XRD, FESEM, TEM, and XPS. The lithium storage performance of the sample was investigated by CV, EIS, and charge/discharge test. The results demonstrated that the $Li_{0.36}V_6O_{13}$ sample exhibited greatly improved electrochemical performance as compared with the pristine V_6O_{13}. For example, when cycled at 0.1 C for 50 cycles, the capacity retention of the $Li_{0.36}V_6O_{13}$ is 97% much higher than that (57%) of the pristine V_6O_{13}. The improvement of the cycle performance of $Li_{0.36}V_6O_{13}$ is attributed to its superior structural reversibility, fewer number of phase transitions during the discharge/charge process, improved electrical conductivity, and enhanced Li^+ diffusivity.

Keywords Lithium-ion batteries · Cathode material · V_6O_{13} · Pre-lithiated · Electrochemical performance

Introduction

Rechargeable lithium-ion batteries (LIBs) are considered one of the most suitable candidates applied for portable electronics because of their high energy density and long-term stability [1–3]. Cathode materials are of great importance for determining the performance of LIBs [4]. Vanadium oxides have been considered to be promising cathode materials for LIBs due to their advantages of high theoretical capacity, high energy density, and wide availability. Vanadium can exist in various valence states (from + 2 to + 5) in vanadium oxides. For example, V_6O_9, V_6O_{13}, V_4O_6, and V_5O_7 have a mixed valence states, while VO_2, V_2O_5, and V_2O_3 have a single valence oxide state [5]. V_6O_{13} has a high theoretical specific capacity of 420 mAh/g, and shows a better electrochemical performance compared with the well-known V_2O_5 [6]. V_6O_{13} consists of alternating layers of single and double vanadium oxide. V^{5+} occupies only the double-layer sites of the V atoms, while V^{4+} occupies the single-layer and double-layer positions of the V atom [7]. The alternating single and double layers provide more lithium intercalation sites [8, 9]. The maximum lithium accommodation is up to eight Li^+ per formula unit theoretically, corresponding to a high theoretical specific capacity and energy of 420 mAh/g [10]. As a mixed-valence vanadium oxide, the preparation of V_6O_{13} is very difficult. On the other hand, the intercalation of lithium into V_6O_{13} lattice leads to volume expansion and structural instability of V_6O_{13}, which would interrupt the electronic and ionic transport paths in the electrodes, and therefore results in rapid capacity decay upon cycling. Moreover, the number of conductive electrons in V_6O_{13} crystal is limited, so its conductivity falls rapidly [11–13]. Pre-lithiation can effectively supplement the consumption of lithium ions during the sealed formation, and improve the capacity and cycle performance of LIBs. Pre-lithiation of cathode material is a very convenient and feasible process. By enriching cathode materials with lithium, the lithium ion can be replenished during the sealed formation, which can control the amount of lithium intercalation and reduce the complexity of the operation, and has important value in actual production [14].

In order to improve its electrochemical properties and electronic conductivity while maintaining its crystal structure, we use a simple solvent-thermal method to obtain pre-lithiated V_6O_{13} cathode materials. The effects of pre-lithiation on the

✉ Zheng-guang Zou
ZhengguangZouglut@163.com

[1] College of Material Science and Engineering, Guilin University of Technology, Guilin 541004, China

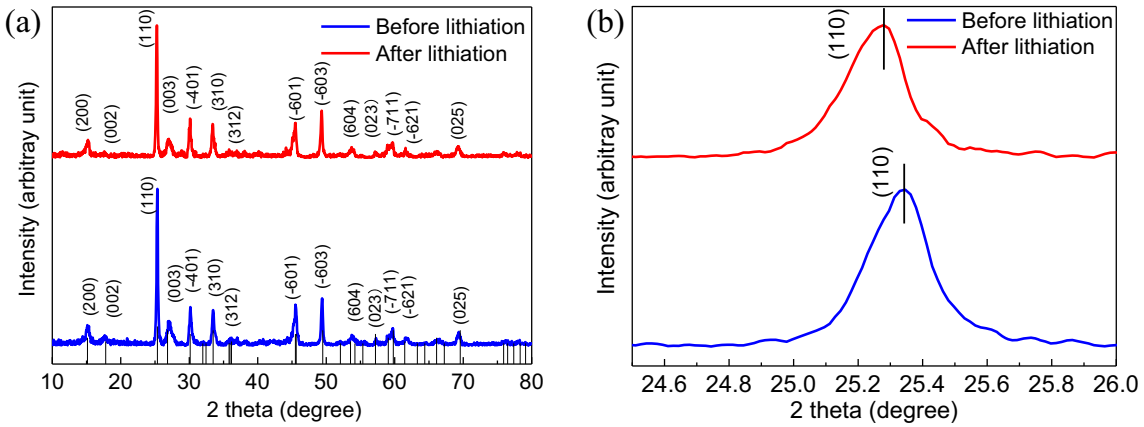

Fig. 1 **a** The XRD patterns of the non-lithiated and pre-lithiated V_6O_{13} and **b** enlarged peaks at 2θ ranging from 24.5 to 26°

microstructure and electrochemical performance of V_6O_{13} were investigated by XRD, XPS, SEM, TEM, CV, EIS, and charge/discharge tests.

Experimental

Material preparation

The pre-lithiated V_6O_{13} was prepared by a facile solvent-thermal method. In a typical synthesis, 0.4 g of V_2O_5 was added to a mixed solution of 25 mL C_2H_5OH and 20 mL deionized water under strong stirring until V_2O_5 was thoroughly mixed. Then, 0.02 g of $LiNO_3$ was dissolved into the mixed solution. The mixed solution was transferred to a 100-mL autoclave, sealed, and kept at 160 °C for 24 h, and then cooled to room temperature. After centrifugation (4000 rpm, 5 min) with deionized water, the sample was freeze-dried for 24 h, ground to a powder, and finally calcined at 350 °C for 1 h at 3 °C/min in argon to obtain the pre-lithiated V_6O_{13}. For comparison, pristine V_6O_{13} was also prepared by the same procedure but without adding $LiNO_3$.

Electrochemical test

The electrochemical performances were measured in coin cells. The working electrodes were prepared by mixing polyvinylidene fluoride (PVDF, 10 wt%), acetylene black (20 wt%), and active materials (70 wt%) in *N*-methyl-2 pyrrolidone (NMP) solvent on an aluminum foil (20 μm in thickness) which was used as the current collectors. The coated electrode was dried in vacuum at 90 °C for 12 h. Both the counter and reference electrodes were commercial Li metal and the separator was the Celgard 2300 membrane. One molar $LiPF_6$ in ethylene carbonate (EC)/dimethyl carbonate (DMC)/diethyl carbonate (DEC) (EC/DMC/DEC = 2:2:1 in volume) was used as electrolyte. The cycling performance was tested by the NEWARE CT-3008 5V 10 mA-164 Battery Testing System (BTS). Both the electrochemical impedance spectroscopy (EIS) and the cyclic voltammetry (CV) were tested through a CHI 860D electrochemical workstation, and the CV measurement was performed in the potential range from 1.5 to 4.0 V at a scan rate of 0.1 mV s^{-1}.

Table 1 The lattice parameters and unit cell volume of pristine V_6O_{13} and pre-lithiated V_6O_{13}

Sample designation	*a* (Å)	*b* (Å)	*c* (Å)	Volume (Å^3)
Pristine V_6O_{13}	11.93209	3.69277	10.13805	438.72
Pre-lithiated V_6O_{13}	11.89303	3.69003	11.0420	479.38

Results and discussion

The XRD pattern of the pristine V_6O_{13} and pre-lithiated V_6O_{13} are showed in Fig. 1a. For the pristine sample, all the diffraction peaks are in accordance with the standard diffraction peaks of the monoclinic phase of V_6O_{13} (JCPDS card no. 71-2235, space group: C2/m) [15]. No impurities are detected from the XRD pattern, indicating high purity of V_6O_{13}. After lithiation, the structure of the main crystal is well remained, but the peak positions slightly shift. Figure 1b shows the enlarged XRD pattern at 2θ ranging from 24.5 to 26°, obviously the (110) peak shifts to low angle after lithiation. The shift of the diffraction peaks indicated that Li^+ had pre-intercalated into the lattice of V_6O_{13}. The lattice parameter values of the two samples were calculated and listed in Table 1. It can be seen that pre-lithiation cause cell volume expansion of V_6O_{13}.

The FESEM and HRTEM images of the pristine V_6O_{13} and pre-lithiated V_6O_{13} samples are shown in Fig. 2. As shown in Fig. 2a and d, both samples have a 3D flower-like structure. By comparison, the pristine V_6O_{13} exhibits more or less agglomeration, and each unit is adhered

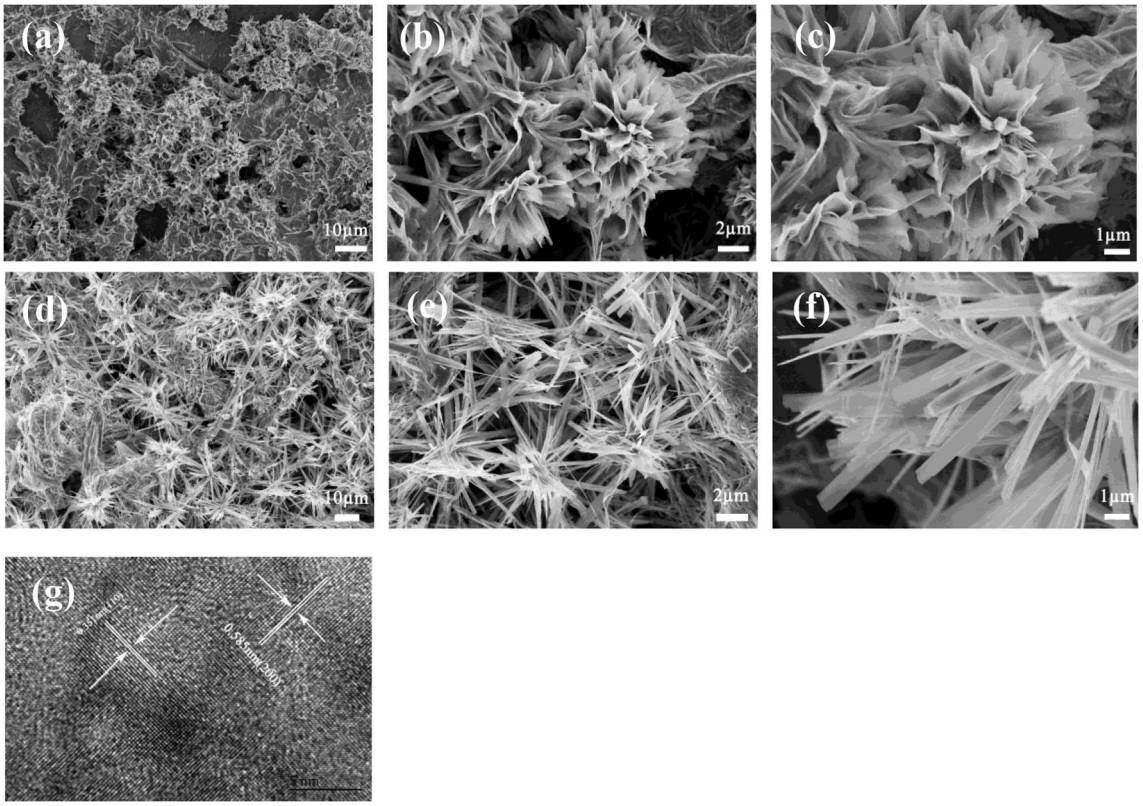

Fig. 2 SEM images of **a**–**c** the pristine V_6O_{13} and **d**–**f** pre-lithiated V_6O_{13}. **g** HRTEM image of the pre-lithiated V_6O_{13}

together in an irregular arrangement. Pre-lithiated V_6O_{13} has less agglomeration, and the flower-like structure of each unit is obvious. In partial magnification of the samples (Fig. 2b, c, e, f), it is seen that the nanoflowers of both samples are composed of very thin 2D nanosheets with smooth surface. After pre-lithiation, the sample "petal" becomes slender, and the nanosheets are looser than the pristine V_6O_{13}. The ample space between each sheet would allow easy penetration of electrolyte [16]. Figure 2g is the HRTEM image of pre-lithiated V_6O_{13}. The lattice fringes are sharp-edged, which means that the pre-lithiated V_6O_{13} has good crystallinity. The 0.351-nm and 0.585-nm lattice fringes correspond to the (110) and (200) lattice planes in the V_6O_{13} structure, respectively.

The composition and the valence state of pre-lithiated V_6O_{13} were investigated by XPS measurement. Figure 3a is XPS survey spectra of the pristine V_6O_{13} and pre-lithiated V_6O_{13}. Due to relatively low content, the characteristic peak of Li is not apparent in the XPS survey spectra. For further verification, the narrow-scan spectra of the pre-lithiated sample were tested (Fig. 3b). After fitting, a distinct characteristic peak at 54.5 eV was observed, corresponding to the Li 1s characteristic peak [17], which provide further evidence for the intercalation of Li into the host lattice. Figure 3c and d are V 2p3/2 and V 2p1/2 XPS spectra of the pristine V_6O_{13} and pre-lithiated V_6O_{13}, respectively. It can be seen that the + 4 and + 5 valence states of vanadium are present in both samples. The binding energy appeared at 522.20, 515.27, 523.69, and 516.29 eV in the sample of pristine V_6O_{13} could be assigned to V^{4+} 2p 1/2, V^{4+} 2p 3/2, V^{5+} 2p 1/2, and V^{5+} 2p 3/2 peaks, respectively [18, 19]. After pre-lithiation, the peak positions of V^{4+} 2p 1/2, $V4^{+}$ 2p 3/2, V^{5+} 2p 1/2, and V^{5+} 2p 3/2 were originated from 522.53, 515.74, 524.01, and 516.67 eV (Table 2). The increase in binding energy of V^{4+} and V^{5+} at the V 2p3/2 peak after pre-lithiation indicates that the lithiating agent leads to an enhanced interaction between vanadium and oxygen atoms [20]. The molar ratios of V^{4+} and V^{5+} of the pristine V_6O_{13} and pre-lithiated V_6O_{13} under the V 2p 3/2 peak are 62.96% and 37.04% (1.7:1) and 65.52% and 34.48% (1.9:1), respectively. It was found that the proportion of V^{4+} increases after pre-lithiation. The increasing fraction of relatively low valence states indicates the reduction of the sample resistance [21].

Figure 4 shows the first three consecutive CV curves of the two samples, at a scan rate of 0.1 mV s^{-1} over a range of 1.5 to 4.0 V (vs. Li/Li^+). For the pristine V_6O_{13}, two oxidation peaks appeared at about 2.60 and 3.25 V, indicating that Li was sequentially deintercalated from the non-equivalent sites in the V_6O_{13} structure. The reduction peaks appeared at about 2.20 V and 2.70 V, corresponding to the intercalation of Li into the monoclinic system

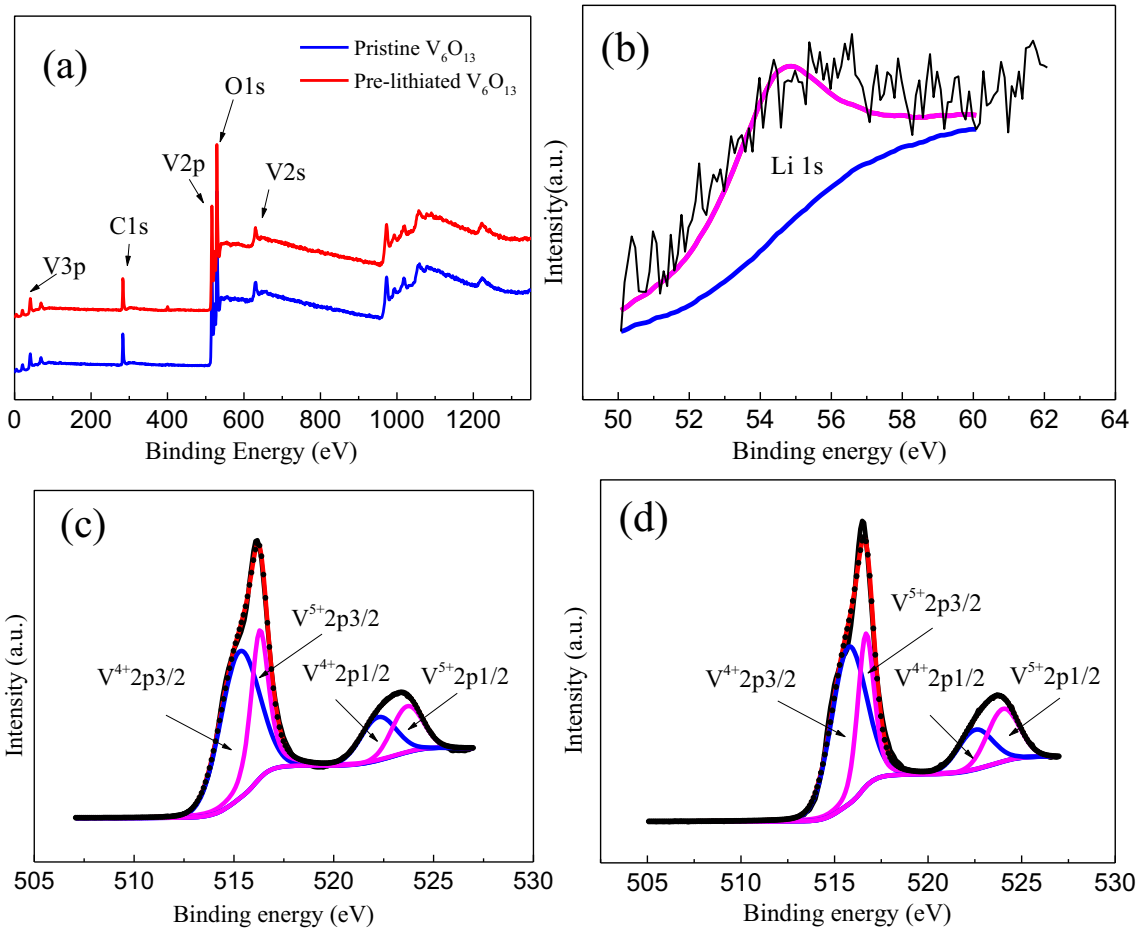

Fig. 3 **a** Overall XPS spectra of the pristine V_6O_{13} and pre-lithiated V_6O_{13}. **b** Li 1s XPS spectra of the pre-lithiated V_6O_{13}. V 2p3/2 and V 2p1/2 XPS spectra of the **c** pristine V_6O_{13} and **d** pre-lithiated V_6O_{13}

V_6O_{13} [22]. The positions of the oxidation peaks and the reduction peaks became narrower after lithiation. The oxidation peaks appeared at about 2.38 V and 2.75 V, and the reduction peaks at about 2.40 V and 2.90 V. The peaks at about 2.75 V and 2.40 V are much higher than those of the pristine V_6O_{13}. An increase in the peak indicates an increase in current, which means that the electron transport of pre-lithiated V_6O_{13} is greatly enhanced [17, 23]. Furthermore, the distinction between the CV curve for the second and third cycles after lithiation and the CV curve for the first cycle is much smaller than for the pristine V_6O_{13}, indicating that the structure is more stable during repeated Li insertion/extraction cycles. The separation between the oxidation peak and the reduction peak after lithiation is minimal, indicating that the reversibility, cyclability, and cycle efficiency of Li^+ insertion/extraction on the electrode are higher [24].

Table 2 The binding energy of V^{4+} and V^{5+} of pristine V_6O_{13} and pre-lithiated V_6O_{13}

Sample	Binding energy (eV)			
	V^{4+} 2p 1/2	V^{4+} 2p 3/2	V^{5+} 2p 1/2	V^{5+} 2p 3/2
Pristine V_6O_{13}	522.20	515.27	523.69	516.29
Pre-lithiated V_6O_{13}	522.53	515.74	524.01	516.67

Figure 5a presents the EIS plots (Z′ vs. -Z″) of the pristine V_6O_{13} and pre-lithiated V_6O_{13} after three cycles. The curves show the depressed semicircles in the high-frequency region and the sloped lines in the low-frequency region, which reflect the charge transfer process and the lithium ion diffusion in the bulk electrode, respectively [25]. The charge transfer resistance of the pristine V_6O_{13} and pre-lithiated V_6O_{13} after 3 cycles was 527.5 Ω and 369.4 Ω, respectively. The charge transfer resistance of lithiation V_6O_{13} is smaller than that of pristine V_6O_{13}, which means that the lithiation V_6O_{13} has higher electrochemical reaction kinetics, which may be because the interlayer spacing of V_6O_{13} increases after pre-lithiation, which facilitates Li^+ insertion/extraction. The diffusion coefficient value (D_{Li}) is calculated using Eqs. (1) and (2) [26].

$$Z' = R_{ct} + RE + \sigma\omega^{-1/2} \quad (1)$$

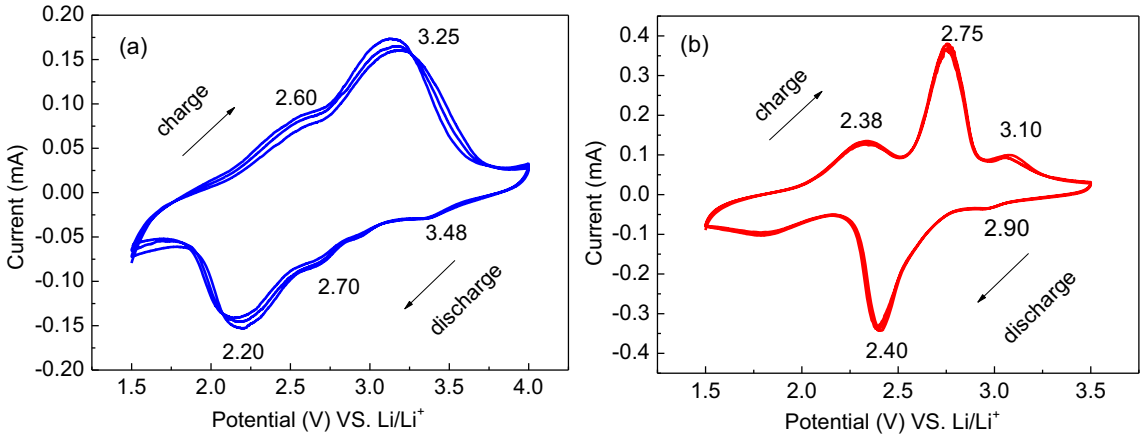

Fig. 4 Cyclic voltammetry curves of **a** pristine V_6O_{13} and **b** pre-lithiated V_6O_{13} with a scanning rate of 0.1 mV s^{-1} in the voltage range of 1.5–4.0 V

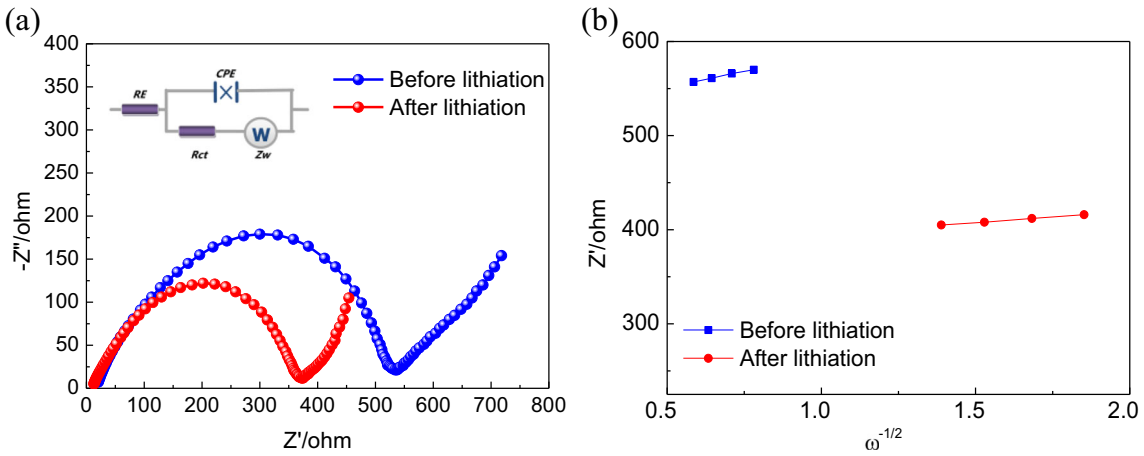

Fig. 5 **a** Nyquist plots of the pristine V_6O_{13} and pre-lithiated V_6O_{13} after the 3rd discharge/charge cycles. **b** The relationship between Z′ and $\omega^{-1/2}$ in the low-frequency range

$$D_{\mathrm{Li}} = \frac{1}{2} \times \left[\left(\frac{Vm}{FS\sigma_{\mathrm{w}}} \right) \frac{dE}{dx} \right]^2 \quad (2)$$

In Eq. (1), ω is the angular frequency in the low-frequency region, and both R_{ct} and RE are kinetics parameters independent of frequency. Then, the Warburg coefficient (σ) can be obtained from the slope of the fitting line (Fig. 5b). In Eq. (2), Vm is the molar volume of cathode material (52 cm^3/mol), F is the Faraday constant (96,485 C/mol), S is the relative area of electrode materials (2 cm^2), σ_{w} is the Warburg impedance, and dE/dx is the value between electromotive force and component. In order to facilitate understanding, the D_{Li} of pristine V_6O_{13} and pre-lithiated V_6O_{13} are 2.72 × 10^{-15} cm^2 s^{-1} and 2.15 × 10^{-14} cm^2 s^{-1}, respectively. The D_{Li} is improved by almost one order of magnitude after pre-lithiation, indicating the faster Li^+ diffusion ability of pre-lithiated V_6O_{13}, which may result from the increased conductivity due to an increase in charge carrier concentration [27, 28]. Table 3 shows the R_{CT} and D_{Li} values of pristine V_6O_{13} and pre-lithiated V_6O_{13}.

Table 3 R_{CT} and D_{Li} values of the pristine V_6O_{13} and pre-lithiated V_6O_{13}

Sample designation	R_{CT} (Ω)	D_{Li} (cm^2 s^{-1})
Pristine V_6O_{13}	527.5	2.72 × 10^{-15}
Pre-lithiated V_6O_{13}	369.4	2.15 × 10^{-14}

Figure 6a and b present selected charge-discharge curves of the pristine V_6O_{13} and pre-lithiated V_6O_{13} at 0.1 C rate in the voltage range of 1.5–4.0 V at room temperature (1 C = 420 mAh/g). The charge and discharge curve of the pristine V_6O_{13} has two obvious discharge plateaus at around 2.0 V and 2.6 V. After lithiation, the discharge voltage increases, and the two plateaus become one plateau (2.7 V), indicating that the polarization of the electrode deceases; moreover, the phase transition numbers are impeded. The decreased phase transition number would be benefit to the improvement of the structural stability of V_6O_{13}. Figure 6c shows the cycling performances of the pristine V_6O_{13} and pre-lithiated V_6O_{13} up to 50 cycles at a current density of 42 mA^{-1} (0.1 C) between 4.0 and 1.5 V.

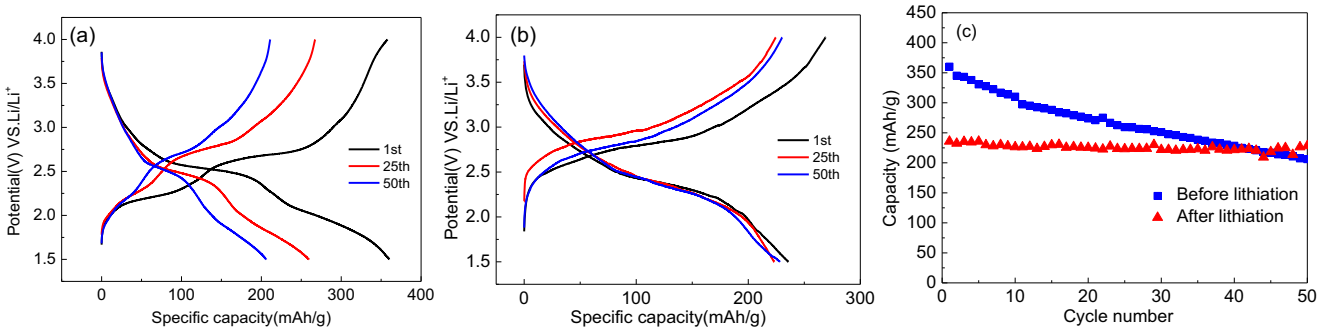

Fig. 6 The first, twenty-fifth, and fiftieth charge-discharge curves of **a** the pristine V_6O_{13} and **b** pre-lithiated V_6O_{13} at 0.1 C rate in the voltage range of 1.5–4.0 V at room temperature. **c** Cycling performance of pristine V_6O_{13} and pre-lithiated V_6O_{13} electrodes at 0.1 C

The initial discharge capacity decay may be caused by the pre-lithiation process, which occupies a large number of Li^+ sites in V_6O_{13} host. Although pre-lithiated V_6O_{13} delivers a lower initial discharge capacity, it exhibits a better cycling performance. The capacity retentions of the pristine V_6O_{13} and pre-lithiated V_6O_{13} after 50 cycles are 57% and 97%, respectively. The improvement of the cycling performance of the pre-lithiated V_6O_{13} is attributed to its superior structural reversibility, lease number of phase transitions during the discharge/charge process, and improved electrical conductivity.

Conclusion

The pre-lithiated V_6O_{13} has been fabricated via a facile solvothermal method. The pre-lithiated V_6O_{13} has a 3D flower-like structure. Electrochemical tests demonstrated that the pre-lithiated V_6O_{13} has a superior electrochemical performance especially the cycling properties. When the mole ratio of Li to V is 0.06, the capacity retention of the sample is 97% after 50 cycles. The improvement of the cycle performance of pre-lithiated V_6O_{13} is attributed to the following reasons: (i) the Li^+ pre-inserted into the lattice structure expand the crystal lattice, which reduces the stress of Li^+ insertion/extraction during charge/discharge; (ii) the fewer number of phase transitions during discharge/charge process therefore led to better cycling stability; (iii) the pre-lithiation process increases the charge carrier concentration, resulting in an increase in conductivity.

Funding information The authors received financial support from the National Nature Science Foundation of China (project no. 51562006).

References

1. Yoo EJ, Kim J, Hosono E, Zhou HS, Kudo T, Honma I (2008) Large reversible Li storage of graphene nanosheet families for use in rechargeable lithium ion batteries. Nano Lett 8:2277–2282
2. Hu LH, Kumar P (2015) Sulphur-reduced self-assembly of flower-like vanadium pentoxide as superior cathode material for Li-ion battery. J Alloys Compd 655:79–85
3. Kumar P, Wu FY, Chou T, Hu LH (2015) Chemically modified morphologies of vanadium pentoxide as superior cathode material for lithium ion battery. J Alloys Compd 632:126–132
4. Wang HL, Yang Y, Liang YY, Robinson JT, Li YG, Jackson A, Cui Y, Dai HJ (2011) Graphene-wrapped sulfur particles as a rechargeable lithium-sulfur-battery cathode material with high capacity and cycling stability. Nano Lett 11:2644–2647
5. Liu J, Xia H, Xue DF, Li L (2009) Double-shelled nanocapsules of V_2O_5 based composites as high-performance anode and cathode materials for Li ion batteries. J Am Chem Soc 131:12086–12087
6. Menetrier M, Levasseur A, Delmas C (1989) Utilization of V_6O_{13} as the positive electrode in lithium batteries. Mater Sci Eng B 3: 103–107
7. Schmitt T, Augustsson A, Nordgren J, Duda LC, Höwing J, Gustafsson T, Schwingenschlögl U, Eyert V (2005) Electronic structure of Li-inserted V_6O_{13} battery cathodes: Rigid band behavior and effects of hybridization, Appl Phys Lett 86 :064101-1-064101-3
8. Li H, He P, Wang Y, Hosono E, Zhou H (2011) High-surface vanadium oxides with large capacities for lithium-ion batteries: from hydrated aerogel to nanocrystalline VO_2(B), V_6O_{13} and V_2O_5. J Mater Chem 21:10999–11009
9. Björk H, Lidin S, Gustafsson T, Thomas JO (2010) Superlattice formation on lithiated vanadium oxide phases $Li_{0.67}V_6O_{13}$ and $Li_1V_6O_{13}$. Acta Crystallogr 57:759–765
10. Höwing J, Gustafsson T, Thomas JO (2010) Low-temperature structure of V_6O_{13}. Acta Crystallogr 59:747–752
11. Xu SX, Cen DC, Gao PB, Huang T, Bao ZH (2018) 3D interconnected V_6O_{13} nanosheets grown on carbonized textile via a seed-assisted hydrothermal process as high-performance flexible cathodes for lithium-ion Batteries. Nanoscale Res Lett 13:1–7
12. Zheng SS, Li XR, Yan BY, Hu Q, Xu YX, Xiao X, Xue HG, Pang H (2017) Transition-metal (Fe, Co, Ni) based metal-organic frameworks for electrochemical energy storage. Adv Energy Mater 7: 1602733
13. Geng PB, Zheng SS, Tang H, Zhu RM, Zhang L, Cao S, Xue HG, Pang H (2018) Transition metal sulfides based on graphene for electrochemical energy storage. Adv Energy Mater 8:1703259
14. Mancini M, Axmann P, Gabrielli G, Kinyanjui M, Kaiser U, Wohlfhrt-Mehrens M (2016) A high-voltage and high-capacity $Li_{1+x}Ni_{0.5}Mn_{1.5}O_4$ cathode material: from synthesis to full lithium-ion cells. Chemsuschem 9:1843–1849
15. Gabrielli G, Marinaro M, Mancini M, Axmann P, Wohlfhrt-Mehrens M (2017) A new approach for compensating the irreversible capacity loss of high-energy Si/C|$LiNi_{0.5}Mn_{1.5}O_4$ lithium-ion batteries. J Power Sources 351:35–44

16. Zhan SY, Wang CZ, Nikolowski K, Ehrenberg H, Chen G, Wei YJ (2009) Electrochemical properties of Cr doped V_2O_5, between 3.8 V and 2.0 V. Solid State Ionics 180:1198–1203
17. West K, Zachau-Christiansen B, Jacobsen T, Atlung S (1985) V_6O_{13}, As cathode material for lithium cells. J Power Sources 14: 235–245
18. Wertheim GK, Attekum PT, Basu S (1980) Electronic structure of lithium graphite. Solid State Commun 33:1127–1130
19. Ichimura K, Sano M (1991) Electrical conductivity of layered transition-metal phosphorus trisulfide crystals. Synth Met 45:203–211
20. Mezentzeff P, Lifshitz Y, Rabalais JW (1990) Compositional and chemical modifications of V_2O_5 and $NaVO_3$ induced by N^{2+} bombardment. Nucl Instrum Methods Phys Res Sect B 44:296–301
21. Lv TT, Zou ZG, Li YW, Li SY, Zhang YJ (2018) Hydrothermal synthesis of high specific capacity Al/Na co-doped V_6O_{13} cathode material for lithium-ion battery. J Electroanal Chem 829:42–50
22. Simões M, Surace Y, Yoon S, Battaglia C, Pokrant S, Weidenkaff A (2015) Hydrothermal vanadium manganese oxides: anode and cathode materials for lithium-ion batteries. J Power Sources 291:66–74
23. Mizuno Y, Hosono E, Saito T, Okubo M, Nishio-Hamane D, Ohishi K, Kudo T, Zhou HS (2012) Electrospinning synthesis of wire-structured LiCoO/r_2/r for electrode materials of high-power Li-ion batteries. J Phys Chem C 116:10774–10780
24. Luo S, Wang K, Wang JP, Jiang K, Li QQ, Fan SS (2012) Binder-free $LiCoO_2$/carbon nanotube cathodes for high-performance lithium ion batteries. Adv Mater 24:2294–2298
25. Chernova NA, Roppolo M, Dillon AC, Whittingham MS (2009) Layered vanadium and molybdenum oxides: batteries and electrochromics. J Mater Chem 19:2526–2552
26. Ding Z, Zhao L, Suo L, Jiao Y, Meng S, Hu YS, Wang Z, Chen L (2011) Towards understanding the effects of carbon and nitrogen-doped carbon coating on the electrochemical performance of $Li_4Ti_5O_{12}$ in lithium ion batteries: a combined experimental and theoretical study. Chem Phys 13:15127–15133
27. Nethravathi C, Rajamathi CR, Rajamathi M, Gautam UK, Wang X, Golberg D (2013) N-doped graphene-VO_2 (B) nanosheet-built 3D flower hybrid for lithium ion battery. ACS Appl Mater Interfaces 5: 2708–2714
28. Chakrabarty DK, Guha D, Biswas AB (1976) Electrical properties of vanadium pentoxide doped with lithium and sodium in the α-phase range. J Mater Sci 11:1347–1353